Numerical Study of Damage in Unsaturated Geological and Engineered Barriers

C. Arson[a], B. Gatmiri[b,c]

[a] *formerly at U.R. Navier, University of Paris-Est (Ecole des Ponts ParisTech) now at Texas A&M University (Texas, USA), Department of Civil Engineering*
[b] *University of Tehran, Department of Civil Engineering*
[c] *formerly at U.R. Navier, University of Paris-Est (Ecole des Ponts ParisTech) now at Agence Nationale pour la Gestion des Déchets Radioactifs (France)*

Abstract

The theoretical framework of a damage model dedicated to non-isothermal unsaturated porous media is presented. The damage variable is a second-order tensor, and the model is formulated in independent state variables. The behavior laws are derived from a postulated expression of Helmholtz free energy. The damaged rigidities are computed by applying the Principle of Equivalent Elastic Energy (PEEE). Internal length parameters are introduced in the expressions of liquid water and vapor conductivities, to account for cracking effects on fluid flows. The damage model has been implemented in Θ-Stock Finite Element program. The mechanical aspect of the damage model is validated by simulating a triaxial compression test on a dry isothermal brittle material. Then, a sophisticated model of nuclear waste disposal, involving two non-isothermal unsaturated porous media, is reproduced. The results obtained in elasticity are in good agreement with the results presented in the corresponding reference article. A parametric study on initial damage is then performed to assess the influence of the Excavated Damaged Zone (EDZ) on the response of the nuclear waste repository during the heating phase. The trends meet the theoretical expectations.

Keywords: damage, suction, temperature, Finite Elements, Excavation Damaged Zone (EDZ)

1. Introduction

This study is motivated by the necessity to predict the behavior of the Excavation Damaged Zone (EDZ) surrounding nuclear waste disposals. The Geological Barriers, often made of quasi-brittle material like granite or clay-rock, undergo damage during the excavation phase. Hydro-mechanical interactions may occur in the neighborhood of the Engineered Barrier, which is generally made of unsaturated compacted clay [1]. Fluids flow inside the gallery. The span of the transient regime depends on the relative values of the involved conductivities [2]. Waste is a heating source which can generate tension, and thus, cracks. The temperature increase tends to reverse the flow of liquid water, and to transform it into vapor at the inner radius of the repository. The complex couplings involved in the geological formation make it necessary to study rock-like quasi-brittle materials as multiphase media. The authors have developed a damage model dedicated to non-isothermal unsaturated porous media [3, 4]. The model, named THHMD model in the following, has been programmed in Θ-Stock Finite Element code [5]. The present article is focused on the numerical validation and justification of the THHMD model. Therefore, only the main modeling assumptions and the most important equations will be exposed in section 2. Then, a numerical validation of the mechanical aspect of the damage model will be presented in section 3. Section 4 contains the main new contribution of this article. Simulations have been performed to model the EDZ at the vicinity of a nuclear waste repository. All the previous results obtained so far with the THHMD model were either focused on mechanics or on flow problems (involving temperature and pore pressure degrees of freedom only). In the simulations presented here, all the degrees of freedom are active and coupled (displacements, temperature, pore pressures). Moreover, the repository model accounts for the interactions between two porous media: the engineered barrier and the geological barrier. The heating phase is simulated in the elastic domain of the damage model, and the results are compared to the results obtained in the corresponding reference article. Then, a parametric study on initial damage is performed to assess the influence of the EDZ on the response of the nuclear waste repository during the heating phase.

2. Outline of the Model

2.1. Variables

Physically, "damaged" means"altered due to the effect of micro-cracks". The constitutive damage model is developed over a Representative Elementary Volume (REV). It is assumed that cracks do not interact. Under this assumption, the loss of elastic deformation energy due to cracking in a REV of volume V containing N cracks is [6]:

$$\Delta W_e \;=\; \frac{8(1-\nu_0^2)}{3(1-\nu_0/2)E_0}\left[(\sigma_{ij}\sigma_{jl})\,\Omega_{li} \;-\; \frac{\nu_0}{2}\sigma_{ji}\,\frac{1}{V}\sum_{K=1}^{N}\left((l^K)^3\,n^K{}_i n^K{}_j n^K{}_p n^K{}_l\right)\sigma_{lp}\right] \tag{1}$$

in which E_0 and ν_0 are the Young's modulus and Poisson's ratio of the undamaged material, respectively. The second-order crack density tensor Ω_{ij} is defined as:

$$\Omega_{ij} \;=\; \frac{1}{V}\Sigma_{K=1}^{N}(l^K)^3\,n_i^K\,n_j^K \tag{2}$$

The K^{th} crack is characterized by a plane orientation (normal vector $\mathbf{n^K}$) and a typical dimension (l^K). The second term of equation 1 represents the effects of the components of crack displacement vectors that are tangential to crack planes. These effects may only be represented by resorting to a fourth order tensor, $\frac{1}{V}\sum_{K=1}^{N}\left(l^{K3}\,n^K{}_i n^K{}_j n^K{}_p n^K{}_l\right)$. However, Kachanov [6] showed that this term could be neglected, so that it is possible to model the degradation of mechanical stiffness due to cracking simply by introducing a second-order damage variable: Ω_{ij} (equation 2). In the present model, the damage variable is defined as the spectral decomposition of the second-order crack density tensor Ω_{ij}. Physically, it means that the cracks contained in the REV are gathered in families, according to their plane orientation. Three principal directions are considered, and therefore, three crack families are defined. As a consequence, damage is expressed in its principal base, and only three equivalent cracks represent all the micro-cracks of the REV. It is assumed that the equivalent cracks are penny-shaped and that a dilatancy coefficient χ relates the crack thicknesses e^k to the crack radii l^k [7]. These geometric assumptions are accounted for to compute the volumetric fraction of the equivalent cracks in the definition of crack density:

$$\Omega_{ij} \;=\; \sum_{k=1}^{3} d^k\,n_i^k\,n_j^k \;=\; \frac{1}{V}\sum_{k=1}^{3}\left(e^k\,\pi\,(l^k)^2\right)\,n_i^k\,n_j^k, \qquad de^k \;=\; \chi\,dl^k \tag{3}$$

The REV is made of a solid skeleton, the pores of which may contain water (in the liquid phase and in the gaseous phase), and air (assumed to be gaseous). The unsaturated porous medium is modeled by requiring to independent state variables. Liquid water and air pore pressures are noted p_w and p_a respectively. Discussing the choice of the stress variable would be beyond the scope of this paper. Formulations in net stress ($\sigma"_{ij} = \sigma_{ij} - p_a\delta_{ij}$) and suction ($s = p_a - p_w$) independent state variables are justified in [8, 9]. Temperature is accounted for by introducing a scalar thermal stress p_T in the thermodynamic variables [4]. Each stress variable is thermodynamically conjugate to a strain variable:

$$\begin{cases} \epsilon_{M_{ij}} \leftrightarrow \sigma"_{ij} \\ \epsilon_{Sv} \leftrightarrow s \\ \epsilon_{Tv} \leftrightarrow p_T \end{cases} \tag{4}$$

in which volumetric strains are denoted with a v subscript. Net stress, suction and thermal stress being independent, the three strain variables mentioned in equation 4 may be used to split the total strain tensor. Assuming that each strain contribution may encompass an elastic (e) and an inelastic (d) part leads to:

$$d\epsilon_{ij} = d\epsilon^e_{M_{ij}} + d\epsilon^d_{M_{ij}} + \frac{1}{3}\delta_{ij}\left(d\epsilon^e_{Sv} + d\epsilon^d_{Sv}\right) + \frac{1}{3}\delta_{ij}\left(d\epsilon^e_{Tv} + d\epsilon^d_{Tv}\right) \tag{5}$$

2.2. Free Energy

The free energy breakdown used by Dragon and his coworkers [10] for damaged dry materials, is generalized and extended to multiphase media:

$$\begin{aligned} \Psi_s(\epsilon_M, \epsilon_{Sv}, \epsilon_{Tv}, \Omega) = {} & \tfrac{1}{2}\epsilon_{M_{ji}} D_{e_{ijkl}}(\Omega)\, \epsilon_{M_{lk}} + \tfrac{1}{2}\epsilon_{Sv}\beta_s(\Omega)\,\epsilon_{Sv} + \tfrac{1}{2}\epsilon_{Tv}\beta_T(\Omega)\,\epsilon_{Tv} \\ & - g_M\,\Omega_{ij}\,\epsilon_{M_{ji}} - \tfrac{g_S}{3}\,\delta_{ij}\,\Omega_{ji}\,\epsilon_{Sv} - \tfrac{g_T}{3}\,\delta_{ij}\,\Omega_{ji}\,\epsilon_{Tv} \end{aligned} \tag{6}$$

$\frac{1}{2}\epsilon_{M_{ji}} D_{e_{ijkl}}(\Omega)\, \epsilon_{M_{lk}}$, $\frac{1}{2}\epsilon_{Sv}\beta_s(\Omega)\,\epsilon_{Sv}$ and $\frac{1}{2}\epsilon_{Tv}\beta_T(\Omega)\,\epsilon_{Tv}$ are the mechanical, capillary and thermal degraded elastic energies respectively. They depend respectively on damaged mechanical, capillary and thermal rigidities ($\mathbf{D_e}(\Omega)$, $\beta_s(\Omega)$ and $\beta_T(\Omega)$ respectively). The capillary rigidity relates suction changes to void ratio changes. The thermal rigidity relates the stress changes due to temperature changes to volumetric deformations. $g_M\,\Omega_{ij}\,\epsilon_{M_{ji}}$, $\frac{g_S}{3}\,\delta_{ij}\,\Omega_{ji}\,\epsilon_{Sv}$ and $\frac{g_T}{3}\,\delta_{ij}\,\Omega_{ji}\,\epsilon_{Tv}$ are residual strain potentials, which quantify the remaining

openings due to cracks after unloading [11]. g_M, g_S and g_T are rigidity-like scalar material parameters that quantify the resistance to crack-closure. The derivation of the free energy $\Psi_s(\epsilon_M, \epsilon_{Sv}, \epsilon_{Tv}, \Omega)$ provides the whole stress/strain relations [3, 4]:

$$\left\{ \begin{array}{l} \sigma"_{ij} \;=\; D_{eijkl}\left(\Omega\right)\,\epsilon_{Mlk} \;-\; g_M\,\Omega_{ij} \\ \\ s \;=\; \beta_s\left(\Omega\right)\epsilon_{Sv} \;-\; \frac{g_S}{3}\,\delta_{ij}\,\Omega_{ji} \\ \\ p_T \;=\; \beta_T\left(\Omega\right)\epsilon_{Tv} \;-\; \frac{g_T}{3}\,\delta_{ij}\,\Omega_{ji} \end{array} \right. \tag{7}$$

For a given sate of damage, incremental stresses are related to the increments of elastic strains as: $d\sigma"_{ij} \;=\; D_{eijkl}\left(\Omega\right)d\epsilon^e_{Mlk}$, $ds \;=\; \beta_s\left(\Omega\right)d\epsilon^e_{Sv}$, $dp_T \;=\; \beta_T\left(\Omega\right)d\epsilon^e_{Tv}$ (for mechanical loadings, this statement is justified in [12]). The incremental inelastic strains $d\epsilon^d_{Mij}$, $d\epsilon^d_{Sv}$ and $d\epsilon^d_{Tv}$ are obtained by: 1. deriving the conjugation relations provided in equations 7, 2. introducing the inelastic strain components (equation 5) in the expression obtained in 1., and 3. combining the resulting relationships with the three latter equalities. As a result, the increments of inelastic strains depend on the increment of damage:

$$\left\{ \begin{array}{l} d\epsilon_{M}{}^d_{ij} \;=\; -D_{eklhg}\left(\Omega\right)^{-1}\,\left(\frac{\partial D_{eghij}(\Omega)}{\partial\Omega_{mn}}\,\epsilon_{Mnm} \;-\; g_M\,Id_{ghij}\right)\,d\Omega_{lk} \\ \\ d\epsilon^d_{Sv} \;=\; -\frac{1}{\beta_s(\Omega)}\left(\epsilon_{Sv}\,\frac{\partial\beta_s(\Omega)}{\partial\Omega_{ij}} \;-\; \frac{g_S}{3}\delta_{ij}\right)\,d\Omega_{ji} \\ \\ d\epsilon^d_{Tv} \;=\; -\frac{1}{\beta_T(\Omega)}\left(\epsilon_{Tv}\,\frac{\partial\beta_T(\Omega)}{\partial\Omega_{ij}} \;-\; \frac{g_T}{3}\delta_{ij}\right)\,d\Omega_{ji} \end{array} \right. \tag{8}$$

To determine the increment of damage, it is necessary to express the damage driving force conjugate to damage (Y_{dij}). The expression of Y_{dij} is deduced from the derivation of the free energy (equation 6):

$$\begin{array}{rl} Y_{d_{ij}} \;=\; -\frac{1}{2}\epsilon_{M_{mn}}\,\frac{\partial D_{e_{nmij}}(\Omega)}{\partial\Omega_{qp}}\,\epsilon_{M_{pq}} \;-\; \frac{1}{2}\epsilon_{Sv}\frac{\partial\beta_s(\Omega)}{\partial\Omega_{ij}}\epsilon_{Sv} \;-\; \frac{1}{2}\epsilon_{Tv}\frac{\partial\beta_T(\Omega)}{\partial\Omega_{ij}}\epsilon_{Tv} & \\ \\ +g_M\,\epsilon_{M_{ij}} \;+\; \frac{g_S}{3}\epsilon_{Sv}\delta_{ij} \;+\; \frac{g_T}{3}\epsilon_{Tv}\delta_{ij} & \end{array} \tag{9}$$

The damage evolution function is assumed to depend on the tensile strains that develop in the skeleton. These latter may be due to mechanical tension

$(g_M\,\epsilon^+_{M_{ij}})$, thermal expansion $(\frac{g_T}{3}\epsilon^+_{Tv}\delta_{ij})$ or pore shrinkage due to suction increase $(\frac{g_S}{3}\epsilon^-_{Sv}\delta_{ij})$. The corresponding thermodynamic variable is noted $Y^+_{d_1\,ij}$ [4, 13]. Like in many models [10, 14, 15] (among others), a very simple damage evolution function is used:

$$f_d\left(Y_{dij},\Omega_{ij}\right) \;=\; \sqrt{\frac{1}{2}\,Y^+_{d_1\,ij}\,Y^+_{d_1\,ji}} \;-\; C_0 \;-\; C_1\,\delta_{ij}\,\Omega_{ji} \tag{10}$$

C_0 is the initial damage-stress rate that is necessary to trigger damage. C_1 controls the damage increase rate. The damage evolution law is computed by an associative flow rule [3, 4].

2.3. Damaged Rigidities

The elastic components of the strain tensor are determined by computing the damaged rigidities $D_{eijkl}\,(\Omega)$, $\beta_s\,(\Omega)$ and $\beta_T\,(\Omega)$. Damaged stress state variables are defined (damaged net stress, damaged suction and damaged thermal stress), by using the fourth-order operator of Cordebois and Sidoroff [16] (noted $M_{ijkl}\,(\Omega)$):

$$M_{ijkl}\,(\Omega)\;\sigma_{lk} \;=\; (\delta-\Omega)^{-1/2}_{ik}\;\sigma_{kl}\;(\delta-\Omega)^{-1/2}_{lj} \tag{11}$$

The Principle of Equivalent Elastic Energy is applied on the three elastic potentials $\frac{1}{2}\epsilon_{M_{ji}}\,D_{e_{ijkl}}\,(\Omega)\;\epsilon_{M_{lk}}$, $\frac{1}{2}\epsilon_{Sv}\beta_s\,(\Omega)\,\epsilon_{Sv}$ and $\frac{1}{2}\epsilon_{Tv}\beta_T\,(\Omega)\,\epsilon_{Tv}$. The final expressions of the damaged rigidities are:

$$\left\{\begin{array}{l} D_{e_{ijkl}}\,(\Omega) \;=\; {M^{-1}}_{ijnm}\,(\Omega)\;D^0_{e_{mnpq}}\,{M^T}_{qpkl}\,(\Omega) \\[2ex] \beta_s\,(\Omega) \;=\; \frac{9\,\beta^0_s}{\left[{(\delta-\Omega)^{-1}}_{ij}\,\delta_{ji}\right]^2} \\[2ex] \beta_T\,(\Omega) \;=\; \frac{9\,\beta^0_T}{\left[{(\delta-\Omega)^{-1}}_{ij}\,\delta_{ji}\right]^2} \end{array}\right. \tag{12}$$

in which $D^0_{e\,ijkl}$, β^0_s and β^0_T are the mechanical, capillary and thermal rigidities in the intact state, respectively.

2.4. Damaged Conductivities

The details of the modeling of thermo-hydraulic transfers in intact unsaturated porous media may be found in [5]. Liquid water flow is governed

by an extended Darcy law, and the model of vapor transfer is inspired from the works of Philip and de Vries [17]:

$$\mathbf{V_w} \;=\; -\frac{\Psi_R\left(\theta_w\right)}{\sigma(T_{ref})}\,\frac{d\sigma(T)}{dT}\,\mathbf{K_w}\cdot\nabla\left(T\right) \;+\; \frac{1}{\gamma_w}\,\frac{\sigma(T)}{\sigma(T_{ref})}\,\mathbf{K_w}\cdot\nabla\left(s\right) \;-\; \mathbf{K_w}\cdot\nabla\left(z\right) \tag{13}$$

$$\mathbf{V^*_{vap}} \;=\; \frac{\rho_{vap}}{\rho_w}\,\mathbf{V_{vap}} \;=\; -D_{T_{vap}}\,\nabla\left(T\right) \;+\; D_{P_{vap}}\,\nabla\left(s\right) \tag{14}$$

$\mathbf{V_w}$ and $\mathbf{V^*_{vap}}$ refer to liquid water and vapor relative velocities, respectively. Ψ_R, which depends on the water content θ_w, has the dimension of a pressure head (in m). It is computed at the reference temperature T_{ref}: $\Psi_R\left(\theta_w\right) = (p_w - p_a)/\gamma_w$. $\sigma(T)$ is the superficial energy of pore water (in $J.m^{-2}$). $D_{T_{vap}}$ and $D_{P_{vap}}$ are the thermal and capillary vapor conductivities, respectively. Only the intrinsic water permeability $\mathbf{K_{int}}\left(n, \Omega_{ij}\right)$, depending on porosity n, is related to the behavior of the solid skeleton:

$$\mathbf{K_w} \;=\; k_T(T)\,k_r(S_w)\,\mathbf{K_{int}}\left(n, \Omega_{ij}\right) \tag{15}$$

The thermal and capillary relative permeabilities $k_T(T)$ and $k_r(S_w)$ are related to heat and to the behavior of pore fluids:

$$k_T(T) \;=\; \frac{\mu_w(T)}{\mu_w(T_{ref})}, \qquad k_r(S_w) = \left(\frac{S_w - S_{w,r}}{1 - S_{w,r}}\right)^3 \tag{16}$$

in which $\mu_w(T)$ is the dynamic viscosity of liquid water, and $S_{w,r}$ is the residual water saturation degree. The water saturation degree S_w evolves on a thermo-hydraulic state surface. This latter is defined by mixing the concept of Bell-shaped space distribution of pores used by Van Genuchten [18] and the assumption of exponential thermal effects done by Gatmiri [5]:

$$\begin{cases} S_w \;=\; \Big[(1 - S_{w,r})\,\left(1 \,+\, (\alpha\, s)^n\right)^{-1+\frac{1}{n}} \,+\, S_{w,r}\Big]\; exp\left(d_s\left(T - T_0\right)\right) \quad if \quad s \geq 0 \\ S_w \,=\, 1 \quad if \quad s < 0 \end{cases} \tag{17}$$

The intrinsic liquid water permeability is split in a reversible part and an irreversible component. The first one quantifies water flow in the reversibly damaged porous matrix, and the second one ($\mathbf{k_2}\left(n^{frac}, \Omega_{rs}\right)$) controls the flow in the cracks network:

$$K_{int_{ij}}\left(n, \Omega_{rs}\right) \;=\; k_{w_0}\,10^{\alpha_w\, e^{rev}}\,\delta_{ij} \;+\; k_{2_{ij}}\left(n^{frac}, \Omega_{ij}\right) \tag{18}$$

k_{w_0} is the reference water permeability of the saturated isothermal porous medium (in $m.s^{-1}$), and e^{rev} is the void ratio of the reversibly damaged porous material. Following Shao's approach [7], $\mathbf{k_2}\left(n^{frac}, \Omega_{rs}\right)$ is computed by assuming that the flow in each micro-crack is laminar. The flow is then homogenized in order to evaluate water transfers in the equivalent cracks damaging the REV:

$$k_{2_{ij}}\left(n^{frac}, \Omega_{rs}\right) \;=\; \frac{\pi^{-2/3}\,\gamma_w}{12\,\mu_w\left(T_{ref}\right)}\,\chi^{4/3}\,b^2\,\sum_{k=1}^{3}\left(d^k\right)^{5/3}\,\left(\delta_{ij} - n_i^k\,n_j^k\right) \tag{19}$$

b plays the role of an internal length parameter, and may be determined if water permeability is known for a certain damage state. In the numerical simulations presented in the following sections, a maximal average damaged permeability K_{wdg}^{max} is used, which is defined as the damaged permeability obtained with 95% isotropic damage: $K_{wdg}^{max} = \frac{1}{3}\delta_{ij}K_{wji}\left(\Omega_{rs} = 0.95\delta_{rs}\right)$. In expression 14, D_{Pvap} and D_{Tvap} both depend on an intrinsic vapor conductivity, which is split in the same manner as the intrinsic water permeability, as:

$$D_{int,\,vap} \;=\; 1.024\,D_0\;n^{rev} \;+\; D_{int,\,vap_2}\left(n^{frac}, \Omega_{rs}\right) \tag{20}$$

A second internal length parameter is introduced in order to compute the damage-related intrinsic vapor conductivity $D_{int,\,vap_2}\left(n^{frac}, \Omega_{rs}\right)$,which is assumed to depend on the mean damage-related water intrinsic permeability:

$$D_{int,\,vap_2}\left(n^{frac}, \Omega_{rs}\right) \;=\; \frac{b^*}{3}\,\delta_{ij}\,k_{2_{ji}}\left(b^*, n^{frac}, \Omega_{rs}\right) \tag{21}$$

b^* is computed by using a maximal damaged vapor conductivity D_{dg}^{max}. Air flow is assumed to be diffusive:

$$\mathbf{V_a} \;=\; -\frac{1}{\gamma_a}\,\frac{p_a \;+\; p_{atm}}{T \;+\; 273.15}\,\mathbf{K_a}\cdot\nabla\left(T(\mathbf{x})\right) - \mathbf{K_a}\cdot\nabla\left(\frac{p_a}{\gamma_a}\right) - \mathbf{K_a}\cdot\nabla\left(z\right) \tag{22}$$

with an air permeability depending on the void ratio e and the saturation degree S_w:

$$\mathbf{K_a} \;=\; c_a\,\frac{\gamma_a}{\mu_a}\;\left[e(1-S_w)\right]^{\alpha_a}\;\vec{\delta} \tag{23}$$

Heat flux is controlled by diffusive, evaporation and convective contributions:

$$\begin{aligned}\mathbf{Q_T} \;=\; &-\lambda_T\,\nabla\left(T\right) \;+\; h_{fg}\,\left(\rho_w\,\mathbf{V^*_{vap}} \;+\; \rho_{vap}\,\mathbf{V_a}\right)\\ &+\;\left[\rho_w\,C_{Pw}\,\mathbf{V_w} \;+\; \rho_w\,C_{Pvap}\,\mathbf{V^*_{vap}} \;+\; \rho_a\,C_{Pa}\,\mathbf{V_a}\right]\,\left(T \;-\; T_0\right)\end{aligned} \tag{24}$$

Only the diffusive component $\lambda_T \nabla(T)$, which involves the solid skeleton, can be influenced by damage. Air and heat diffusive flow directions are assumed not to be affected by the fracture network. The expressions of the corresponding conductivities are thus kept unchanged from the intact configuration. The influence of damage is quantified by the total porosity, which depends on total volumetric strains, and thus, on inelastic strain components. Damage is also accounted for through the degree of saturation, which depends on suction, and thus, on damaged water conductivities.

2.5. Experimental Determination of the New Material Parameters

The undamaged capillary rigidity β_s^0 (respectively thermal rigidity β_T^0) may be determined by oedometric tests under suction control (respectively under temperature control). The damage material parameters that have been introduced in the THHMD model are: the damage evolution parameters (C_0 and C_1), the resistances to crack closure (g_M, g_S and g_T), the dilatance parameter χ and the two internal lengths b and b^*. Halm and Dragon set up triaxial compression tests that enable the determination of C_0, C_1 and g_M [19]. Such tests can be adapted to get g_S and g_T. χ has been measured in rocks by Shao's research team [7]. b may be identified by percolation tests [20, 21]. These tests have to be adapted to get the internal length related to vapor flow (b*) [17]. In its present state, the model resorts to maximum damaged conductivities (K_{wdg}^{max} and D_{dg}^{max}). Indeed, it is easier to determine conductivity in a cracked medium than to identify an internal length experimentally. K_{wdg}^{max} and D_{dg}^{max} are the conductivities measured when the material is reaching failure, for a conventional isotropic damage of 0.95%. Introducing the conventional damage value and the maximum conductivities in equations 19 and 21 makes it possible to compute b and b*.

3. Assessment of Mechanical Damage at the Lab Scale

The aim of the simulation presented in this section is to validate the mechanical representation of damage proposed in the THHMD model. The validation has already been done successfully on granite, which is a material of interest for nuclear waste disposals [4]. The purpose of this section is to bring new evidence of the capabilities of the model, by extending the mechanical validation to another geomaterial. A triaxial compression test performed on a cylindrical sandstone sample is simulated. The input parameters of interest for this simulation are provided in Table 1. The values

Table 1: Main Material Parameters used to Simulate the Triaxial Compression Test on Vosges Sandstone.

E (Pa)	ν	e_0	g_M (Pa)	C_0 (Pa)	C_1 (Pa)
$1.17 * 10^{10}$	0.2	0.2658	$-3.2 * 10^7$	$2 * 10^4$	$2.7 * 10^5$

are taken from the reference study of Dragon's research team [10]. e_0 is the initial void ratio of the material. In this study, the material is assumed to be dry, so that the pore pressure degrees of freedom are set to zero during the simulation. The test is isothermal, so that the temperature degree of freedom is neutralized as well. Damage can only affect the mechanical rigidity and strains of the sample. The cylinder is 4 cm high and the radius is 2 cm. Only one half of the longitudinal section of the sample is modeled, in axis-symmetric conditions. The boundary conditions are the following:

- vertical displacements fixed to zero at the bottom ($u_z = 0$)
- radial displacements fixed to zero on the axis ($u_r = 0$)
- external lateral boundary subjected to a constant confining pressure $p_c = 15\,MPa$
- top boundary condition subjected to a varying compressive load ($\sigma_{zz} = p_c$ during the confining phase, and $\sigma_{zz} = p_c + \sigma_{load}$ in the compression phase).

The match between numerical results and experimental reference data is very satisfactory, as can be seen from Fig. 1.a. Axial compression generates lateral tensile strains, developing equally in r- and θ- directions. This is the reason why there is no axial damage ($\Omega_{zz} = 0$) and this is also the reason why both lateral components of damage are equal during all the test (Fig. 1.b). Damage grows with deviatoric stress, which reflects the corresponding growth of radial and orthoradial tensile strains. Damage predictions are thus consistent with the theoretical formulation of the model and with the mechanical loading at stake in this test.

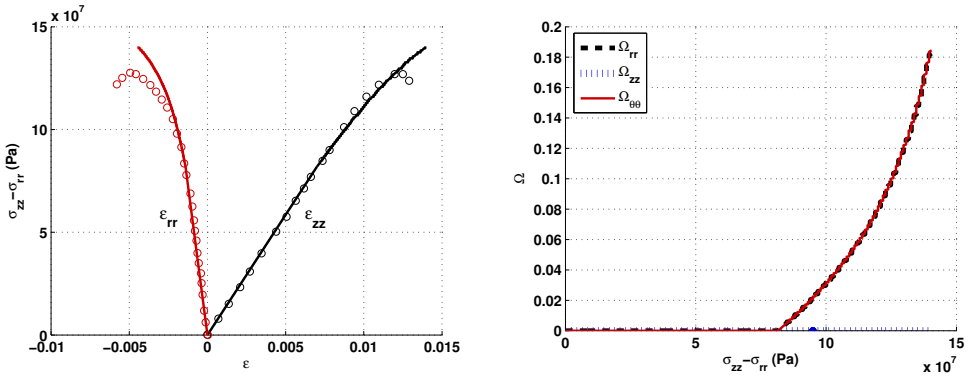

a. b.

Figure 1: Triaxial Compression Test on Vosges Sandstone ($p_c = 15MPa$). a. Strain Evolution (dots: experimental results, solid lines: numerical results). b. Damage Evolution.

4. Coupled Heat and Fluid Flows in the EDZ

4.1. Presentation of the FE Model

The following study is based on the works of Gens's research team on FEBEX project [1]. The objective is to model nuclear waste disposals. Nuclear waste is stored in cylindrical canisters, the radius of which is 0.465m. A bentonite buffer, 0.7m thick, surrounds the container. The packages are stored horizontally, in boreholes realized from a deep gallery excavated in granite. The space between canisters is assumed to be large enough to neglect group effects. An axis-symmetric numerical model is designed to study the influence of the heating power of nuclear waste on the Engineered Barrier (i.e. the bentonite buffer) and on the Geological Barrier (i.e. the granite massif). The massif is studied over a large distance from the canister, equal to one hundred times the thickness of the bentonite buffer (i.e. r=70m). The model is pseudo-one-dimensional: the thickness of the studied sections of bentonite and granite is 0.7m long, which is one hundred times lower than the model's width. The aim of this study is to contribute to the validation of the integration of the THHMD model in Θ-Stock, and then, to justify the use of the THHMD model to study the Excavation Damaged Zone (EDZ). First, results obtained in elasticity are compared with the results provided by Gens et al. [1]. Then, a parametric study is performed to assess the influence of initial damage in the granite massif, which may be cracked during the excavation of the gallery, before the heating phase.

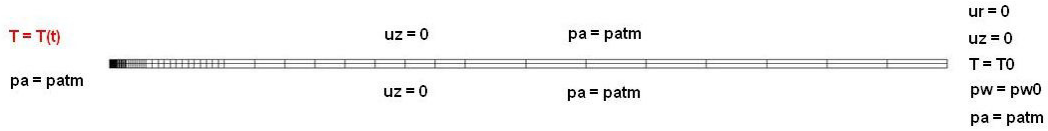

Figure 2: Mesh and Boundary Conditions Adopted to Simulate the Heating Phase in a Nuclear Waste Disposal.

The initial conditions are the following:

- initial stress state: $\sigma_{rr} = \sigma_{zz} = \sigma_{\theta\theta} = 5\,MPa$ in bentonite, zero initial stress in granite
- initial temperature in both materials: $12\,^oC$
- initial air pressure in both materials: $p_{atm} = 10^5\,Pa$
- water pressure initialized by inverting the formula of the retention curve, from the value of the initial degree of saturation: $S_{w0} = 0.46$ in bentonite, $S_{w0} = 1$ in granite.

The boundary conditions adopted for all the simulations are summarized on Fig. 2. The temperature imposed at the left boundary (contact surface between the canister and the bentonite buffer) varies as follows:

- the temperature is raised from 12^oC to 100^oC in 21 days
- then, the temperature is maintained at 100^oC during 3 years (which sets the end of this stage at 1095 days)
- the temperature is decreased exponentially in time during 6 months (which sets the end of this stage at 1278 days).

All the simulations presented here are performed in elasticity (thus, $g_M = g_S = g_T = 0$). In the parametric study, the EDZ is represented by setting a non zero damage tensor in the initial state, for selected granite elements. Most of the material parameters are provided in the reference article [1]. According to the formula adopted by Gens et al. for the state surface of the

Table 2: Main Material Parameters used to model the Granite Bedrock.

E (Pa)	ν	β_s^0 (Pa)	β_T^0 (Pa)	e_0
$3.51 * 10^{10}$	0.3	$2.92 * 10^{11}$	$2.92 * 10^{11}$	0.0101
$S_{w,r}$	$\alpha_{VG}\,(Pa^{-1})$	n_{VG}	$d_s\,(^oC^{-1})$	
0	10^{-5}	1.5	0	
$k_{w0}\,(m.s^{-1})$	α_w	χ	$k_{wdg}^{max}\,(m.s^{-1})$	
10^{-11}	0	0.005	10^{-7}	
c_a	α_a	$D_{dg}^{max}\,(m^2.s^{-1})$		
$10^{-10}\,m^2$	0	10^{-5}		
λ_s	λ_w	λ_a	h_{fg}	α_T
$(W.m^{-1}.^oC^{-1})$	$(W.m^{-1}.^oC^{-1})$	$(W.m^{-1}.^oC^{-1})$	$(J.kg^{-1})$	$(^oC^{-1})$
3.6	0.6	0.0258	$2.5\,10^6$	$-7.8 * 10^{-6}$
C_{Ps}	C_{Pw}	C_{Pvap}	C_{Pa}	
	$(J.kg^{-1}.^oC^{-1})$			
793	4180	1900	1006	

void ratio, the intact capillary rigidity β_s^0 is proportional to the bulk modulus. Gens et al. also use retention curves obtained with a Van Genuchten model [18], but without temperature couplings (thus, $d_s = 0$). The internal length parameters are computed by assuming that K_{wdg}^{max} and D_{dg}^{max} are respectively 10000 times and 100 times higher than the intrinsic water permeability. The thermal conductivity curve is fitted to the one obtained in Gens et al.'s model to get the thermal conductivity of the solid phases. α_T refers to the thermal expansion coefficient of the solid grains. More details on the choice of the material parameters provided in Tables 2 and 3 are available in [13].

4.2. Heating Test in an Undamaged Geological Formation

The problems studied here involves four simultaneous flows: liquid water flow, vapor flow, dry air flow and heat flow. Each transfer is characterized by a specific time scale, wich makes it difficult to choose the time step size that has to be adopted in the successive loading phases. The authors are still working on time step optimization to avoid oscillation phenomena, like those observed in Fig. 3 and 5. Radial displacement trends are in agreement with the results obtained by Gens (Fig. 3). The bentonite buffer expands during

Table 3: Main Material Parameters used to model the Bentonite Buffer.

E (Pa)	ν	β_s^0 (Pa)	β_T^0 (Pa)	e_0
$2.60 * 10^7$	0.3	$2.17 * 10^9$	$2.17 * 10^8$	0.6846
$S_{w,r}$	$\alpha_{VG}\,(Pa^{-1})$	n_{VG}	$d_s\,(^oC^{-1})$	
0	$2 * 10^{-8}$	2	0	
$k_{w0}\,(m.s^{-1})$	α_w	χ	$k_{wdg}^{max}\,(m.s^{-1})$	
10^{-13}	0	0.005	10^{-9}	
c_a	α_a	$D_{dg}^{max}\,(m^2.s^{-1})$		
$10^{-10}\,m^2$	0	10^{-7}		
λ_s	λ_w	λ_a	h_{fg}	α_T
$(W.m^{-1}.^oC^{-1})$	$(W.m^{-1}.^oC^{-1})$	$(W.m^{-1}.^oC^{-1})$	$(J.kg^{-1})$	$(^oC^{-1})$
1.05	0.6	0.0258	$2.5\,10^6$	-10^{-5}
C_{Ps}	C_{Pw}	C_{Pvap}	C_{Pa}	
	$(J.kg^{-1}.^oC^{-1})$			
1091	4180	1900	1006	

the heating phase, and shrinks during the relaxation period. The orders of magnitude are respected, but the displacements are about three times higher with Θ-Stock in bentonite. This may be explained by the difficult parameter setting for this material. Gens et al. modeled the mechanical behavior of bentonite by a state surface controlling the evolution of the void ratio. In Θ-Stock, a linear elastic model governs the mechanical part of the behavior, and it seems that the bentonite modeled with Θ-Stock is less stiff than in Gens et al.'s study. Consequently, the granite bedrock is less loaded than expected, which explains why the radial displacements in the geological formation are less important in the simulation performed with Θ-Stock than in Gens et al.'s reference study. The evolution of temperature is well-reproduced even in the transient stage (Fig. 4), despite the thermal conductivity model is different from the one used in the reference study. The trends of water pressure and of the degree of saturation in the contact zone between both barriers are satisfactory (Fig. 5), even if the desaturation of the bentonite buffer after the heating phase is more important in Θ-Stock computations. This discrepancy may be attributed to the complex couplings involved in the THHMD model, which make it difficult to fit all the retention parameters, especially when two porous media interact. Generally speaking,

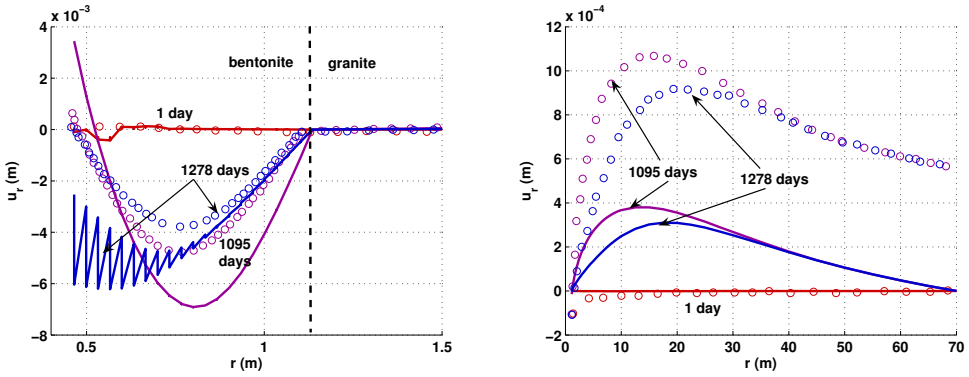

a. b.

Figure 3: Radial displacements in the Engineered (a.) and Geological (b.) Barriers. Dots: reference results from [1]. Solid lines: results obtained with Θ-Stock in the elastic domain of the THHMD model.

the behavior of the Engineered and Geological Barriers are well-represented, which justifies a study more focused on damage.

4.3. Heating Test in a Bedrock Damaged by the Excavation

The purpose of the following simulations is to study the influence of the Excavation Damaged Zone (EDZ) on the response of the Engineered and Geological Barriers. It is assumed that it is possible to forecast the mechanical damage induced by excavation. This is justified from the results obtained in the previous section, which gave evidence that the THHMD model can reproduce mechanical damage in porous media. The aim of the following investigation is to perform a parametric study on the influence of initial damage in an elastic, non-isothermal, unsaturated granite massif. This is justified from the results obtained in the previous paragraph, which showed that the subroutines implemented in Θ-Stock for the THHMD model enabled couped thermo-hydro-mechanical studies on elastic media. The mesh, material data, initial and boundary conditions are the same as in the previous paragraph.

The influence of initial damage is studied by setting a non zero, isotropic damage state on the elements of the granite formation which are relatively close to the excavation: $R_b \leq r \leq 4R_b$, in which R_b is the radius of the bentonite buffer. The presence of cracks in the Geological Barrier lowers the mechanical, capillary and thermal rigidities of granite, which explains why

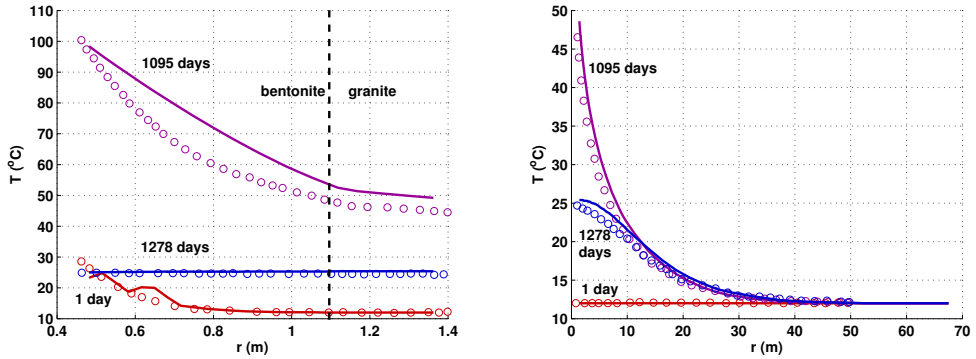

a. b.

Figure 4: Temperature in the Engineered (a.) and Geological (b.) Barriers. Dots: reference results from [1]. Solid lines: results obtained with Θ-Stock in the elastic domain of the THHMD model.

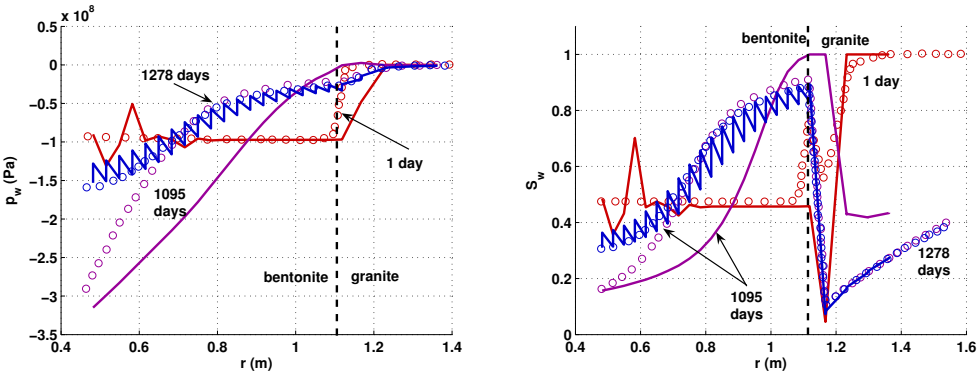

a. b.

Figure 5: Water pressure (a.) and degree of saturation (b.) in the Engineered Barrier. Dots: reference results from [1]. Solid lines: results obtained with Θ-Stock in the elastic domain of the THHMD model.

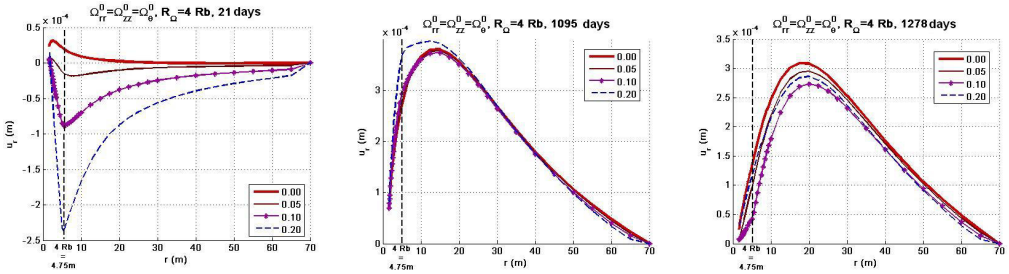

a. b. c.

Figure 6: Influence of initial isotropic damage on radial displacement in the whole barrier after a. 21 days, b. 1095 days, c. 1278 days.

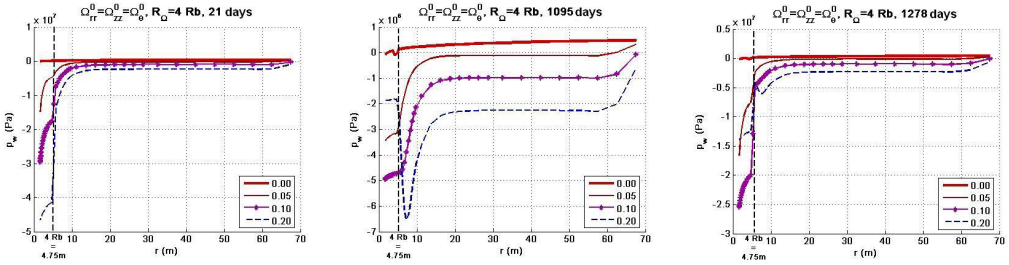

a. b. c.

Figure 7: Influence of initial isotropic damage on water pressure in the whole barrier after a. 21 days, b. 1095 days, c. 1278 days.

the amplitude of radial displacements generally increases with initial damage (Fig. 6). Damage also increases water conductivities in the granite bedrock, which becomes more affected by the suction effects occurring in the bentonite buffer. Contrary to the reference case with an undamaged bedrock, the damaged Geological Barrier tends to desaturate (Fig. 7 and 8). This does not affect much the saturation degree of the bentonite buffer, but this results in a tremendously lower degree of saturation of the granite bedrock at the vicinity of the canister (Fig. 9).

5. Conclusion

A damage model dedicated to non-isothermal unsaturated porous media is presented. Following the assumption of non-interacting cracks, the damage variable is expressed as the spectral decomposition of the second-order crack density tensor. The model is formulated in mechanical, capillary and

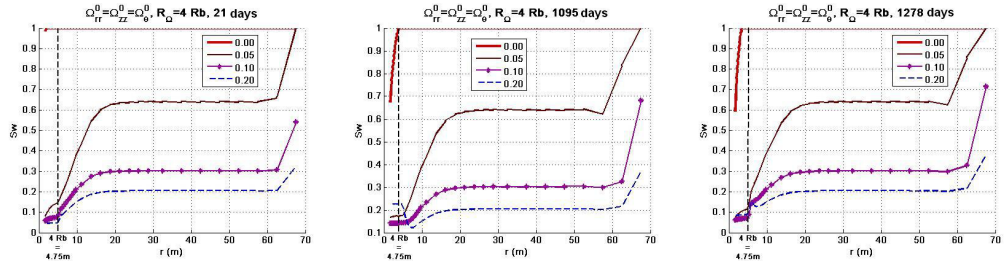

a. b. c.

Figure 8: Influence of initial isotropic damage on the degree of saturation in the whole barrier after a. 21 days, b. 1095 days, c. 1278 days.

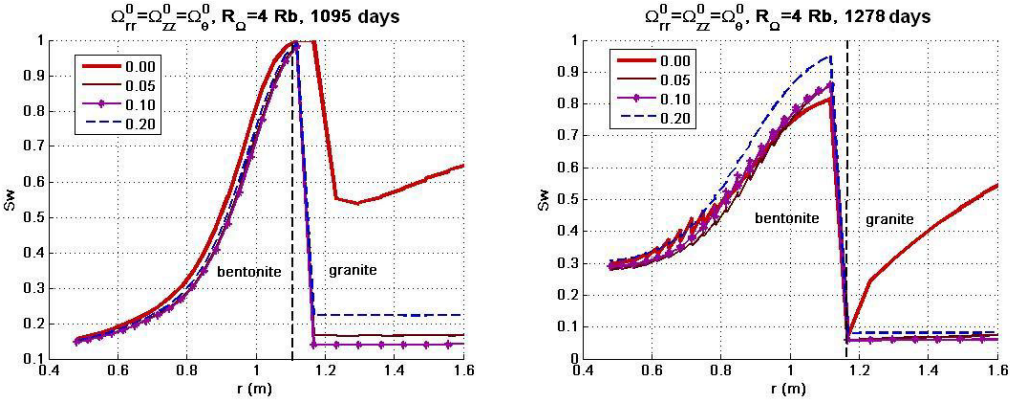

a. b.

Figure 9: Influence of initial isotropic damage on the degree of saturation at the frontier between the Engineered Barrier and the Geological Barrier after a. 1095 days, b. 1278 days.

thermal independent state variables. Correspondingly, Helmholtz free energy is split in three thermodynamic potentials, each of which being the sum of a degraded elastic energy and of a residual strain potential. This latter enables the representation of remaining crack openings after unloading without requiring an additional plastic potential. The increment of damage is determined by an associated flow rule. The damage evolution function represents the growth of damage with tensile mechanical strains, compressive capillary strains and tensile thermal strains. The damaged mechanical, capillary and thermal rigidities are computed by applying the Principle of Equivalent Elastic Energy (PEEE). Cracking effects are also accounted for in the transfer rules. Specific conductivities, related to internal length parameters, are introduced in the transfer equations for liquid water and vapor. This is aimed at modeling the orientation and intensity changes induced by cracking in fluid flows. Air and heat conductivities depend on volumetric strains and on the degree of saturation, which depend in turn on damage.
A triaxial compression test performed on a dry isothermal brittle material is simulated. The match with the experimental reference data is excellent. This first simulation thus validates the ability of the damage model to represent the degradation of the mechanical rigidity with cracking. Then, an elaborate model of nuclear waste disposal is reproduced. It involves two non-isothermal unsaturated porous media. The heating phase is simulated in the elastic domain of the damage model, and the results are compared to the ones presented in the corresponding reference study. The comparison shows that the program implemented for the damage model enables the representation of complex thermo-hydro-mechanical couplings. This justifies the use of the damage model to study the influence of the Excavation Damage Zone surrounding the repository. A parametric study on initial damage is performed to this purpose. The results are in agreement with the theoretical assumptions done to develop the model regarding the physical phenomena at stake. These very encouraging achievements will be completed to perform further analyses on coupled effects generating cracking (mechanical, capillary and thermal damage), on the combination of various time and space scales, and on the long-term effects of damage.

Acknowledgement

This research has been supported by the European project TIMODAZ (*Thermal Impact on the Damaged Zone Around a Radioactive Waste Dis-*

posal in Clay Host Rocks), launched by EURATOM (*European Community of Atomic Energy*).

References

[1] A. Gens, A. Garcia-Molina, S. Olivella, E. Alonso, F. Huertas, Analysis of a full scale in situ test simulating repository conditions, International Journal for Numerical and Analytical Methods in Geomechanics 22 (1998) 515–548.

[2] K. Pruess, J. Wang, Y. Tsang, On thermohydrologic conditions near high-level nuclear wastes emplaced in partially saturated fractured tuff. 2. effective continuum approximation., Water Resources Research 26 (1990) 1249–1261.

[3] C. Arson, B. Gatmiri, A mixed damage model for unsaturated porous media, Comptes-Rendus de l'Académie des Sciences de Paris, section Mécanique 337 (2009) 68–74.

[4] C. Arson, B. Gatmiri, Numerical study of a thermo-hydro-mechanical model for unsaturated porous media, Annals of Solid and Structural Mechanics 1 (2010) 59–78.

[5] B. Gatmiri, C. Arson, Theta-stock, a powerful tool for thermohydromechanical behaviour and damage modelling of unsaturated porous media, Computers and Geotechnics 35 (2008) 890–915.

[6] M. Kachanov, Effective elastic properties of cracked solids: critical review of som basic concepts, Appl. Mech. Rev. 45 (8) (1992) 304–335.

[7] J. Shao, H. Zhou, K. Chau, Coupling between anisotropic damage and permeability variation in brittle rocks, International Journal for Numerical and Analytical Methods in Geomechanics 29 (2005) 1231–1247.

[8] D. Fredlund, N. Morgenstern, Stress state variables for unsaturated soils, J. of the Soil Mechanics and Foundations Division (1977) 447–466.

[9] G. Houlsby, The work input to an unsaturated granular material, Gotechnique 47 (1) (1997) 193–196.

[10] A. Dragon, D. Halm, T. Désoyer, Anisotropic damage in quasi-brittle solids: modelling, computational issues and applications, Comput. Methods Appl. Mech. Engrg. 183 (2000) 331–352.

[11] G. Swoboda, Q. Yang, An energy-based damage model of geomaterials 1. formulation and numerical reults, Int. J. Solids and Struct. 36 (1999) 1719–1734.

[12] R. AbuAlRub, G. Voyiadjis, On the coupling of anisotropic damage and plasticity models for ductile materials, International Journal of Solids and Structures 40 (2003) 2611–2643.

[13] C. Arson, Etude théorique et numérique de l'endommagement thermo-hydro-mécanique des milieux poreux non saturés, Ph.D. thesis, Ecole Nationale des Ponts et Chaussées, Paris (2009).

[14] F. Homand-Etienne, D. Hoxha, J. Shao, A continuum damage constitutive law for brittle rocks, Computers and Geotechnics 22 (2) (1998) 135–151.

[15] J. Shao, N. Ata, O. Ozanam, Study of desaturation and resaturation in brittle rock with anisotropic damage, Engineering geology 81 (2005) 341–352.

[16] J. Cordebois, F. Sidoroff, Endommagement anisotrope en lasticit et plasticit, Journal de Mcanique thorique et applique (special issue) (1982) 45–60.

[17] J. Philip, D. de Vries, Moisture movement in porous materials under temperature gradients, Transactions, American Geophysical Union 38 (2) (1957) 222–232.

[18] M. VanGenuchten, A closed-form equation for predicting the hydraulic conductivity of unsaturated soils, Soil Science Society of America Journal 44 (1980) 892–898.

[19] D. Halm, A. Dragon, Modélisation de l'endommagement par mésofissuration du granite, Revue Française de Génie Civil 17 (2002) 21–33.

[20] Y. Guéguen, P. Gravilenko, M. L. Ravalec, Scales of permeability, Surveys in Geophysics 17 (1996) 245–263.

[21] G. Zimmermann, H. Burkhardt, L. Engelhard, Scale dependence of hydraulic and structural parameters in the crystalline rock of the ktb, Pure Appl. Geophys. 160 (2003) 1067–1085.